SCIENCE CHINA
Technological Sciences

October 2013 Vol.56 No.10: 2586–2593
doi: 10.1007/s11431-013-5306-2

Phase-field simulation of dendritic growth in a forced liquid metal flow coupling with boundary heat flux

DU LiFei*, ZHANG Rong & ZHANG LiMin

School of Science, Key Laboratory of Space Applied Physics and Chemistry, Ministry of Education, Northwestern Polytechnical University, Xi'an 710072, China

Received May 4, 2013; accepted July 4, 2013; published online August 27, 2013

A phase-field model with forced liquid metal flow was employed to study the effect of boundary heat flux on the dendritic structure forming of a Ni-40.8%Cu alloy with liquid flow during solidification. The effect of the flow field coupling with boundary heat extractions on the morphology change and distributions of concentration and temperature fields was analyzed and discussed. The forced liquid flow could significantly affect the dendrite morphology, concentration and temperature distributions in the solidifying microstructure. And coupling with boundary heat extraction, the solute segregation and concentration diffusion were changed with different heat flux. The morphology, concentration and temperature distributions were significantly influenced by increasing the heat extraction, which could relatively make the effect of liquid flow constrained. With increasing the initial velocity of liquid flow, the lopsided rate of the primary dendrite arm was enlarged and the transition of developing manner of the secondary arms moved to the large heat extraction direction. It was the competition between heat flux and forced liquid flow that finally determined microstructure forming during solidification.

phase-field simulation, liquid flow, heat flux, solidification

Citation: Du L F, Zhang R, Zhang L M. Phase-field simulation of dendritic growth in a forced liquid metal flow coupling with boundary heat flux. Sci China Tech Sci, 2013, 56: 2586–2593, doi: 10.1007/s11431-013-5306-2

1 Introduction

Mechanical properties of materials are strongly dependent upon their multi-scale microstructures that form during manufacturing processes such as solidification, heat treatment, etc. To improve materials performance, it is valuable to understand the key factors affecting the microstructure formation. As it is very difficult to observe the detailed evolution process of microstructure formation experimentally, computer simulations have drawn great attentions in modeling of multi-scale structure formation and its effect on mechanical properties [1]. For decades, phase-field method has become a popular technique to model various types of complex microstructure formation and evolution during materials processing as well as mechanical loading, such as solidification, spinodal decomposition, Ostwald ripening, crystal growth and recrystallization, domain microstructure evolutions in ferroelectric materials, martensitic transformation, dislocation dynamics, crack propagation, etc. [2–5] Using phase-field method to simulate the solidification process has been widely reported in the past two decades. Kobayashi [6] developed a simple phase-field model for one component melt growth including anisotropy, and used this model to study the formation of various dendritic patterns. He found the qualitative relations between the shapes of crystals and some physical parameters and that noises gave a crucial influence on the side branch structure of dendrites. The phase-field model for alloys was firstly developed by Wheeler et al. [7, 8], which is called the WBM model. Kim et al. [9, 10] presented another model for alloys by adopting

*Corresponding author (email: dulifei@mail.nwpu.edu.cn)

the thin interface limit, which is known as the KKS model. Karma [11, 12] presented a phase-field formulation to simulate quantitatively microstructural pattern formation in alloys, and the thin-interface limit of this formulation yielded a much less stringent restriction on the choice of interface thickness than previous formulations and permitted one to eliminate non-equilibrium effects at the interface. Dendrite growth simulations with vanishing solid diffusivity showed that both the interface evolution and the solute profile in the solid were accurately modeled by this approach. Recently, solidifications with forced flow or convection were studied in binary alloys in 2D and 3D. Beckermann et al. [13] developed a novel diffusion interface model for the direct numerical simulation of microstructure evolution in solidification processes involving convection in the liquid phase. In their model, solidification front was treated as a moving interface in the diffuse approximation. They used their models to simulate the coarsening of a mush of a binary alloy and the dendritic growth in the presence of melt convection. Lan et al. [14] carried out the efficient adaptive phase-field simulation for a non-isothermal free dendritic growth in a nickel/copper system with a forced liquid flow. From the study, they found that a steady-state growth could be obtained quickly and the calculated solution agreed quite well with the Oseen-Ivontsov solution in isothermal condition. Also, solidifications of multi-component and multiphase were also studied using phase-field methods [15−17].

However, solidification microstructure depends on many technical conditions, such as the fluid flow, heat and mass transfer as well as interfacial and kinetic phenomena, so it is significant to study the effect of these conditions on the microstructure formation process, in order to find the way of solidification process control to carry out the materials design. So in this study, we will employ a non-isothermal phase-field model, coupling with liquid flow and heat extraction from boundary, to study the effect of heat extraction on the concentration and temperature diffusion during the liquid-solid phase transition in the interface region with a forced liquid flow, which can result in the microstructure and concentration change in metal alloys.

2 Modeling and simulation method

The phase-field model for non-isothermal simulation of binary systems [18, 19] was combined with the Beckerman's model for solidification with convection [13, 14] to study the flow field effect on the convection and temperature distribution during dendritic growth. The main governing equations are listed below:

Phase-field equation

$$\frac{\partial \phi}{\partial t}=M_\phi \bar{\varepsilon}^2\left[\nabla\cdot\left(\eta^2\nabla\phi\right)-\frac{\partial}{\partial x}\left(\eta\eta_\beta^{'}\frac{\partial \phi}{\partial y}\right)+\frac{\partial}{\partial y}\left(\eta\eta_\beta^{'}\frac{\partial \phi}{\partial x}\right)\right] - M_\phi\left(\left(1-x_{\mathrm{B}}\right)H_{\mathrm{A}}+x_{\mathrm{B}}H_{\mathrm{B}}\right). \tag{1}$$

Diffusion equation

$$\frac{\partial x_{\mathrm{B}}}{\partial t}+\boldsymbol{V}\cdot\nabla C = \nabla\cdot D\left[\nabla x_{\mathrm{B}}+\frac{V_m}{R}x_{\mathrm{B}}\left(1-x_{\mathrm{B}}\right)\left(H_{\mathrm{A}}\left(\phi,T\right)-H_{\mathrm{B}}\left(\phi,T\right)\right)\nabla\phi\right]. \tag{2}$$

Temperature equation

$$c_p\left(\frac{\partial T}{\partial t}+\boldsymbol{V}\cdot\nabla T\right)+30g\left(\phi\right)\Delta\tilde{H}\dot{\phi}=\nabla\cdot K\nabla T. \tag{3}$$

Continuity equation

$$\nabla\cdot\left(\phi\boldsymbol{V}\right)=0. \tag{4}$$

Momentum equation

$$\frac{\partial \phi\boldsymbol{V}}{\partial t}+\phi\boldsymbol{V}\cdot\boldsymbol{V}=-\frac{\phi}{\rho}\nabla P+\nu\nabla^2\left(\phi\boldsymbol{V}\right)+\boldsymbol{M}_{\mathrm{d}}. \tag{5}$$

In this model, the phase-field variable ϕ varies smoothly between 0 in the solid and 1 in the liquid as we assumed, x_{B} is the mole fraction of solute B in solvent A and T is the temperature. ϵ is the coefficient of gradient energy, which is determined by the interfacial energy. The anisotropy is included in the system because the phase change kinetics depends upon the orientation of the interface. Here, we introduce the anisotropy by $\epsilon=\bar{\varepsilon}\eta=\bar{\varepsilon}\left(1+\gamma\cos k\beta\right)$, where $\bar{\varepsilon}$ is related to the surface energy σ and interface thickness λ, γ is the magnitude of anisotropy in the surface energy, κ specifies the mode number and the expression β=arctan(ϕ_y/ϕ_x) gives an approximation of the angle between the interface normal and the orientation of the crystal lattice. V, P, ρ, and v are the liquid velocity, pressure, density, and kinematic viscosity, respectively.

The formulations included in these governing equations are

$$H_{\mathrm{A}}\left(\phi,T\right)=W_{\mathrm{A}}g'\left(\phi\right)+30g\left(\phi\right)\Delta H_{\mathrm{A}}\left(\frac{1}{T}-\frac{1}{T_m^{\mathrm{A}}}\right), \tag{6}$$

$$H_{\mathrm{B}}\left(\phi,T\right)=W_{\mathrm{B}}g'\left(\phi\right)+30g\left(\phi\right)\Delta H_{\mathrm{B}}\left(\frac{1}{T}-\frac{1}{T_m^{\mathrm{B}}}\right), \tag{7}$$

$$\breve{c}=\left(1-x_{\mathrm{B}}\right)c_{\mathrm{A}}+x_{\mathrm{B}}c_{\mathrm{B}}, \tag{8}$$

$$\Delta\tilde{H}=\left(1-x_{\mathrm{B}}\right)\Delta H_{\mathrm{A}}+x_{\mathrm{B}}\Delta H_{\mathrm{B}}, \tag{9}$$

$$K=\left(1-c_{\mathrm{B}}\right)K_{\mathrm{A}}+x_{\mathrm{B}}K_{\mathrm{B}}, \tag{10}$$

$$\boldsymbol{M}_{\mathrm{d}}=-\frac{\nu b\left(1-\phi\right)^2\phi\boldsymbol{V}}{\lambda^2}, \tag{11}$$

where $g(\phi)=\phi^2(1-\phi)^2$ and W_A, W_B are constants, T_m^A and T_m^B are the melting point of pure A and pure B, respectively. ΔH_A and ΔH_B are the heats of fusion per volume, c_A and c_B are the heat capacities and R is the gas constant. $p(\phi)$ is a smoothing function, chosen such that $p'(\phi)=30g((\phi))$. The diffusion coefficient is postulated as a function of the phase- field variable, $D=D_s+p(\phi)(D_L-D_S)$, where D_S and D_L are the classical diffusion coefficients in the solid and liquid, respectively.

These governing equations were solved using the standard finite difference methods with the Tri-diagonal matrix algorithm (TDMA) and time stepping is by explicit Euler scheme. To solve the velocity field, we used the SIMPLE (Semi-Implicit Method for Pressure-Linked Equations) algorithm. In 2D simulations, the velocity field can be evaluated by solving eq. (5) with expanding $\boldsymbol{V}$ to $\boldsymbol{V}(U,V)$,

$$\frac{\partial U}{\partial t}=-\frac{U}{\phi}\frac{\partial \phi}{\partial t}-\left(\frac{\partial U^2}{\partial x}-\frac{\partial(UV)}{\partial y}\right)-\frac{1}{\rho}\frac{\partial P}{\partial x}+\nu\left[\left(\frac{\partial^2 U}{\partial x^2}+\frac{\partial^2 U}{\partial y^2}\right)+\frac{U}{\phi}\nabla^2\phi\right]-\frac{\nu b(1-\phi)^2 U}{\delta^2}, \quad (12)$$

$$\frac{\partial V}{\partial t}=-\frac{V}{\phi}\frac{\partial \phi}{\partial t}-\left(\frac{\partial V^2}{\partial y}-\frac{\partial(VU)}{\partial x}\right)-\frac{1}{\rho}\frac{\partial P}{\partial y}+\nu\left[\left(\frac{\partial^2 V}{\partial x^2}+\frac{\partial^2 V}{\partial y^2}\right)+\frac{V}{\phi}\nabla^2\phi\right]-\frac{\nu b(1-\phi)^2 V}{\delta^2}. \quad (13)$$

The pressure correction equation is

$$P'_{i,j}=-a^{-1}\left[b\left(P'_{i+1,j}+P'_{i-1,j}\right)+c\left(P'_{i,j+1}+P'_{i,j-1}\right)+d\right], \quad (14)$$

where

$$a=2\Delta t\left(\frac{1}{\Delta x^2}+\frac{1}{\Delta y^2}\right), \quad (15)$$

$$b=-\frac{\Delta t}{\Delta x^2}, \quad (16)$$

$$c=-\frac{\Delta t}{\Delta y^2}, \quad (17)$$

$$d=\nabla\cdot\boldsymbol{V}=\frac{1}{2\Delta x}\left(U_{i+1,j}-U_{i-1,j}\right)+\frac{1}{2\Delta y}\left(V_{i,j+1}-V_{i,j-1}\right). \quad (18)$$

The boundary with different heat fluxes is chosen in the temperature-field calculation. The boundary heat flux can be introduced as $Q=\lambda_i(\partial T/\partial x)$ at left boundary [20], as shown in Figure 1, the density of the heat flux at boundaries is the control parameter, which determines the magnitude and direction of the heat flux. Because of the symmetry, we initially added a solid nucleus at the left domain (600×1200 units) wall, and simulated the growth of a single solid seed in this two-dimensional simulation box filled with undercooled melt. Interfacial energy exhibits 4-fold anisotropy in all simulations. The boundary conditions are shown in Figure 1, and the initial input liquid flow is from the top to the bottom. The zero-flux condition was used for both concentration and temperature, but the result was the same due to the large domain used. All the other parameters we used in our simulations can be found in refs. [18, 19], and they were collected in Table 1.

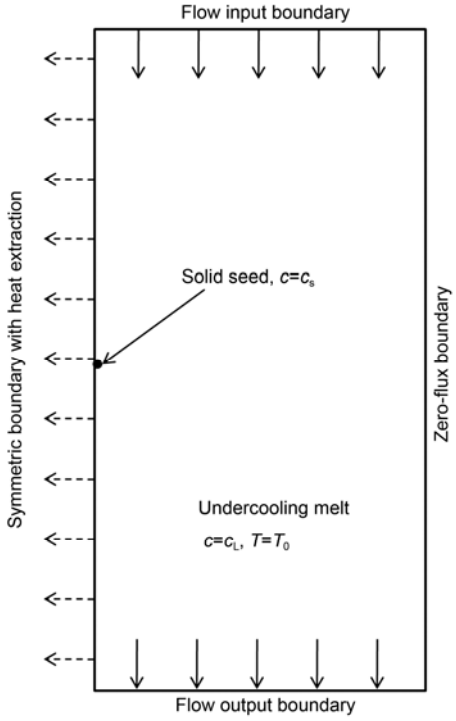

Figure 1 A schematic of simulation zone.

Table 1 Thermophysical parameters used in simulations

Parameter	Value
Melt temperature of Ni (K)	1728.0
Melt temperature of Cu (K)	1358.0
Latent heat of Ni (J m^{-3})	2.35×10^9
Latent heat of Cu (J m^{-3})	1.728×10^9
Heat conductivity of Ni (W mK^{-1})	84.0
Heat conductivity of Cu (W mK^{-1})	200.0
Specific heat of Ni (J m^{-3}K^{-1})	5.42×10^6
Specific heat of Cu (J m^{-3}K^{-1})	3.96×10^6
Diffusion coefficient of the liquid phase (m^2 s^{-1})	1.0×10^{-9}
Diffusion coefficient of the solid phase (m^2 s^{-1})	1.0×10^{-13}
Mole volume of alloy (m^3 mol^{-1})	7.42×10^{-6}
Surface energy of Ni (J m^{-2})	0.37
Surface energy of Cu (J m^{-2})	0.29
Interfacial energy coefficient of Ni (m sK^{-1})	3.3×10^{-3}
Interfacial energy coefficient of Cu (m sK^{-1})	3.9×10^{-3}

3 Results and discussion

Figure 2 showed the concentration distribution maps of dendritic structure forming in the forced metal liquid flow of 0.05 m s^{-1}, heat flux of different values was applied at the left boundary in these simulations to present heat extractions at different levels during phase-transition, the corresponding temperature distribution maps were plotted in Figure 3, and morphology maps were similar to the concentration maps. Without heat flux at boundary, as shown in Figure 2(a), the dendrite showed an unsymmetrical microstructure in the upstream and downstream regions with force liquid flow introduced at the initial. Dendritic arms grew fast towards the liquid flow in the upstream region, but the secondary arms were hard to form in horizontal direction. While in the downstream region, dendritic structure forming was significantly suppressed in both horizontal and vertical directions, the velocity of the primary dendrite growth is much smaller than that in the upstream region and few secondary arms were formed. Solute diffusion also showed different influence, liquid flow enhanced the solute diffusion in the upstream region and formed thinner solute diffusion layer, but in downstream the solute segregation was significantly enhanced with thick diffusion layer.

The temperature map in Figure 3(a) indicated that temperature in the upstream region was higher than that in the downstream region, but the dendritic structure forming was enhanced with small undercooling with liquid flow introduced. Heat flux from boundary could directly change the temperature distribution in simulation regions, thus affecting dendrite growth process. With heat extraction from left boundary, the whole dendritic structure forming was significantly enhanced with increasing of heat flux. Secondary dendrite arms started to form with heat extraction from left boundary, and by increasing heat flux, much more secondary arms formed and grew towards horizontal direction in

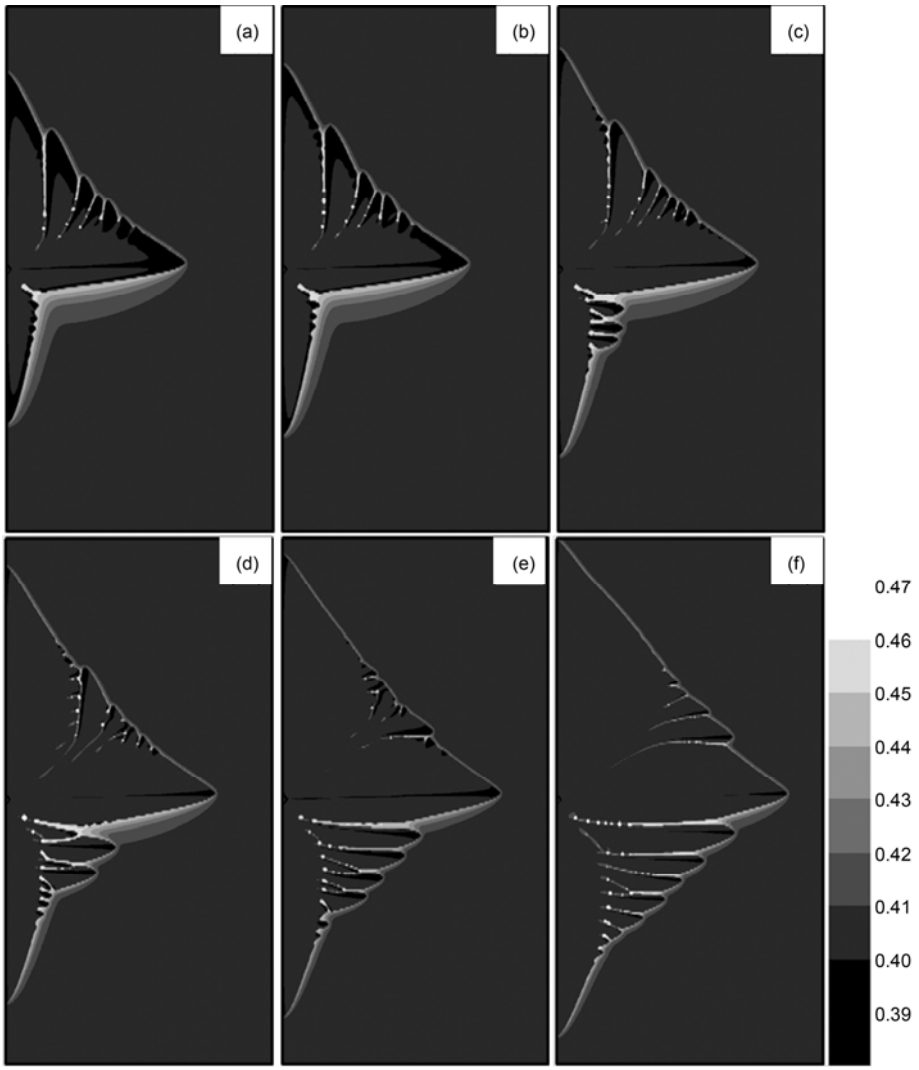

Figure 2 Concentration distribution maps at time=1.5 ms. The initial liquid flow velocity is 0.05 m s^{-1}, and the heat extraction from boundary is (a) 0; (b) 2.0×10^{-3} W m^{-2}; (c) 6.0×10^{-3} W m^{-2}; (d) 10.0×10^{-3} W m^{-2}; (e) 14.0×10^{-3} W m^{-2}; (f) 18.0×10^{-3} W m^{-2}, respectively.

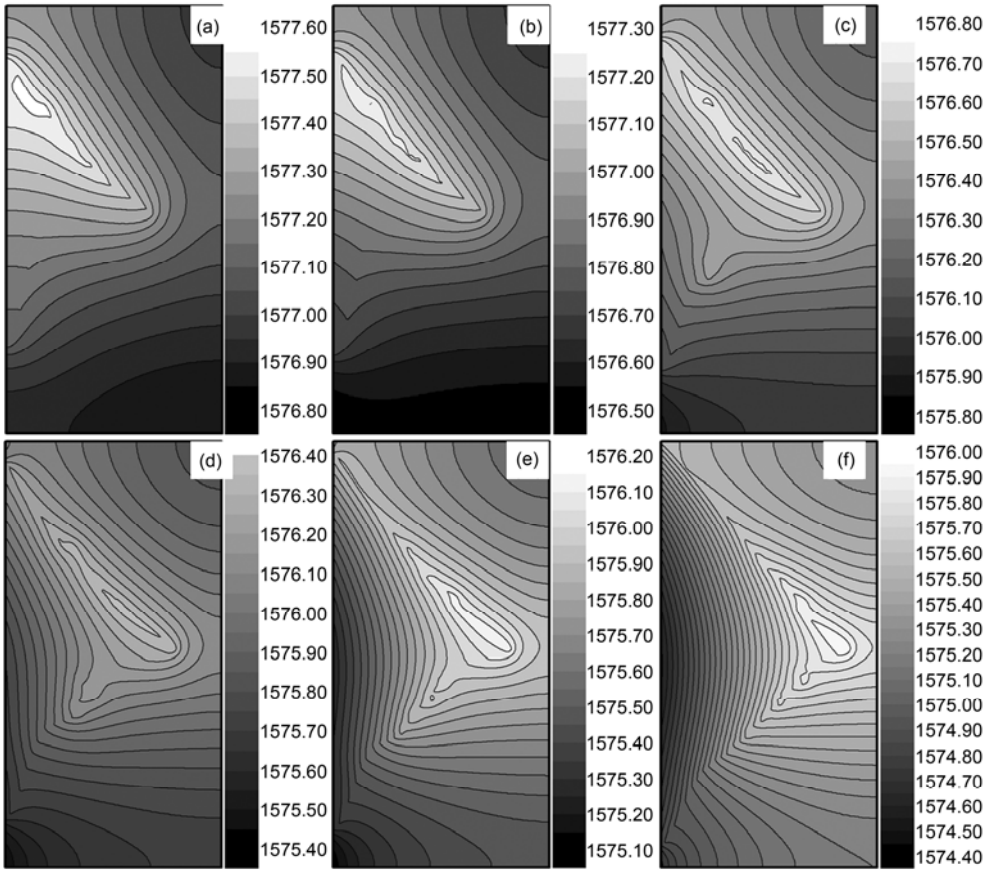

Figure 3 Temperature distribution maps at time=1.5 ms. The initial liquid flow velocity is 0.05 m s^{-1}, and the heat extraction from boundary are (a) 0; (b) 2.0×10^{-3} W m^{-2}; (c) 6.0×10^{-3} W m^{-2}; (d) 10.0×10^{-3} W m^{-2}; (e) 14.0×10^{-3} W m^{-2}; (f) 18.0×10^{-3} W m^{-2}, respectively.

the downstream region. While in upstream, the secondary arms became compressed due to the coarsening of the primary arms caused by large undercooling, and with intense increasing of the heat extraction, secondary arms growing towards vertical direction disappeared, and new secondary arms growing towards horizontal direction began to form. Solute diffusion also showed significant changes with heat extractions from boundary. Phase transition was enhanced with large undercooling caused by heat extraction and rapid solidification led to weak solute segregation in both upstream and downstream regions especially that solute diffusion layer in the downstream region became thinner with increase of heat flux. These changes of solute diffusion led to the different concentration distributions inside dendrite microstructure, large heat extraction from boundary made the distribution difference inside dendrite structure constrained with rapid phase-transition under large undercoolings. In Figure 4(a), we plotted the concentration distribution profiles along left boundary with different heat extractions. Solute segregation in the downstream region was constrained as the result of temperature distribution changes as shown in Figure 4(b), but the enhanced changes took place in the downstream region.

Figure 3 indicated that, by increasing the heat flux, there was an obvious change in the temperature distribution. With small heat extraction from left boundary, the temperature distribution was mostly affected by latent heat release from liquid-solid phase transition, so temperatures in the upstream region were higher because of rapid solidification caused by the forced liquid flow, which made an irregular distribution. With the increase of heat extraction from left boundary, the effect of latent heat release during solidification on temperature rising was relatively weakened, and heat extraction became the main factor that determined the temperature distribution, thus the temperature map became symmetry with large enough heat extraction (Figure 3(f)). These changes in temperature distributions also had an influence on solidification velocities.

The tip velocities of primary dendrite arms growing into downstream and upstream regions with different heat flux were plotted in Figure 5. With small heat extractions, the tip velocity kept decreasing because of the temperature rising caused by latent heat release as we discussed in the temperature distribution in Figure 3. But with intense heat extraction from boundary, there was a velocity increasing at the early primary arm growing, but the velocity was decreased with time evolution, this effect could be found in both downstream and upstream regions. And comparing the dendrite

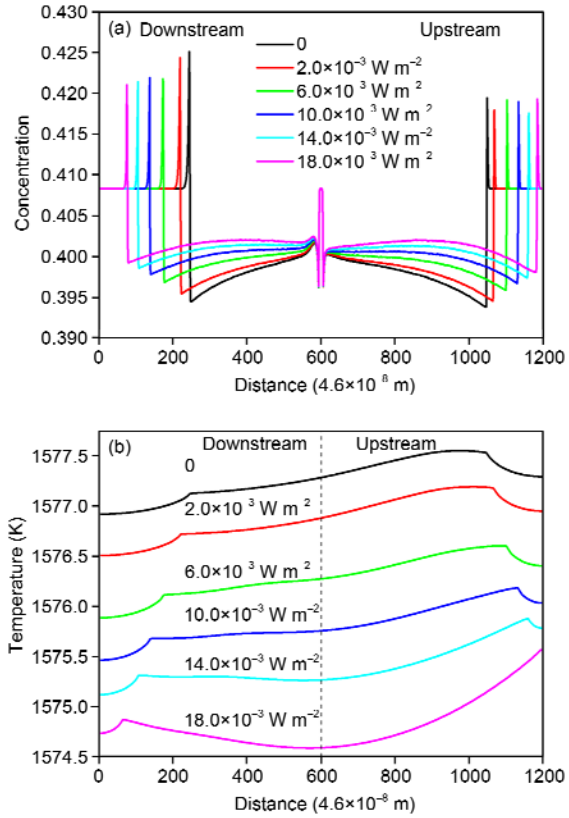

Figure 4 Concentration and temperature distribution profiles along left boundary with different heat extractions from boundary.

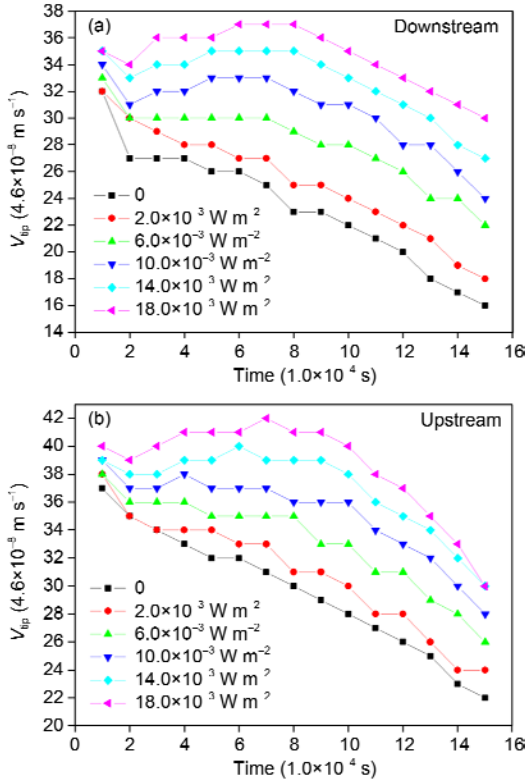

Figure 5 Tip velocities of dendritic primary arms with different heat extractions from boundary.

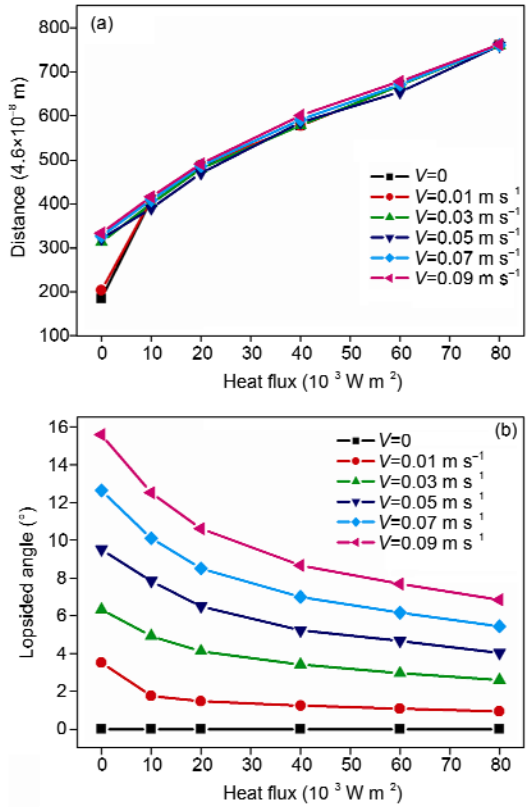

Figure 6 Tip positions and lopsided angle of horizontal dendritic primary arm varying with different initial flow velocities heat extractions from boundary.

growth in the downstream and upstream regions, the tip growth of primary arm growing in the upstream region was faster than that in the downstream region with different heat extractions, and tip growth in both downstream and upstream regions was enhanced by increasing the heat extraction, but heat flux increasing had a relatively large influence on tip growth in the downstream region, which could lead to the approximately symmetry structure forming as shown in Figure 2(f) with large heat extraction from boundary. We calculated the tip difference between the tip velocity in the downstream and upstream regions, and found that, the tip growth in the upstream region was fast due to force liquid flow, but with large heat extraction from boundary, the tip growing velocity in downstream could be equal to that in the upstream region, as shown in line with λ=18.0×10^{-3} W m^{-2}.

As shown in Figure 2, the primary arm growing in horizontal direction was lopsided due to the forced liquid flow introduced at the initialization, and different initial flow velocities had different influences on the microstructure forming in vertical direction [14]. In addition, with heat extractions from left boundary, the growth of this primary arm was also enhanced in the horizontal direction, so there should exist a growth competition between thermal and convective dendrites, and it was necessary to examine the lopsided angle change caused by the heat flux as well as velocity of initial liquid flow. In Figure 6, we gave tip

positions and lopsided angles of horizontal dendritic primary arm at t=2.0 ms varying with different heat extractions from boundary and initial flow velocities.

With the same initial liquid flow, the tip moving velocity in vertical direction was not changed with different heat flux, but the tip position in horizontal direction, as plotted in Figure 6(a), was significantly increased with large heat flux, so the lopsided angle decreased with increasing heat extraction from left boundary, which was plotted in Figure 6(b), and it was obvious that large heat flux could restrain the effect of liquid flow on the microstructure changes. With the increase of the velocity of the initial liquid flow, the tip moving velocity in vertical direction was enhanced with large liquid flow, and the lopsided angle became large, but increasing the heat extraction could still lead to the decrease of the lopsided angle due to the large growing speed of the primary arm as the result of the large undercooling caused by the heat extraction.

From the microstructure evolution during the solidification in the forced liquid flow with heat extractions, we can find that there was a transition of developing manner of the secondary arms with increasing the heat extraction at the boundary, and with increasing initial liquid flow, this secondary arms developing manner transition occurred at different levels, so we plotted a diagram of secondary arms developing manner transition map in Figure 7 by carrying out simulations with different heat extraction and initial liquid flow. With small heat extraction flux and large velocity of initial liquid flow, the microstructure was dendrite, and secondary arm forming was enhanced in the upstream with secondary arm suppressed in the downstream. With large heat extraction flux and small initial velocity of initial liquid flow, the microstructure became columnar, and when the heat extraction was large enough, the steady state should be columnar structure. There was also the transition state with mix-structure of dendrite and columnar, and with increase of initial velocity of initial liquid flow, this transition state could be moved to the large heat extraction direction with the scale of this state increased. Therefore, the heat extraction flux and liquid flow together led to the final macrostructure forming in the direction solidification.

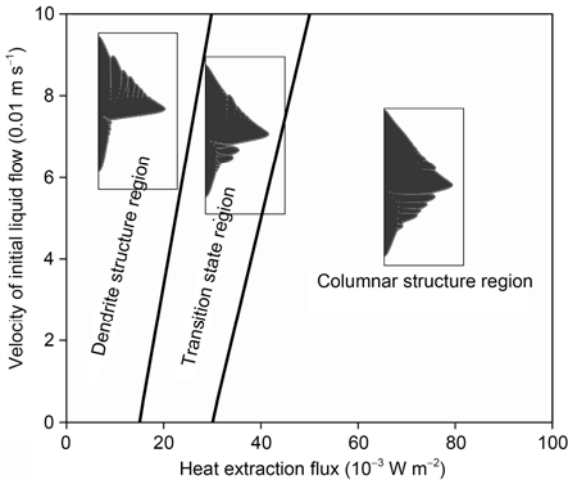

Figure 7 Microstructure transition map for directional solidification with different initial liquid flow and heat extraction at boundary.

4 Conclusions

Liquid metal flow is a common phenomenon in castings, as known, it has a significant influence on the morphology formation, concentration and temperature distributions during directional solidification, also, different heating treatment could cause microstructural changes during phase transitions. In this study, we used a non-isothermal phase-field model coupling with forced liquid metal flow to investigate the effect of liquid flow on the microstructure forming of a Ni-40.8%Cu alloy with boundary heat flux during solidification. A forced liquid metal flow was introduced at the initial stage, and different levels of heat flux were set at simulation boundary to present heat treatment at the chilling walls. The effect of the flow field coupling with boundary heat extractions on the distributions of composition and temperature fields was analyzed and discussed. Forced liquid flow could significantly affect dendrite morphology, concentration and temperature distributions. With the introduced heat extraction, temperature distribution changed significantly, which could lead to changes of solute diffusion and solidification microstructure. Large heat flux at boundary could significantly influence the morphology, concentration and temperature distributions, which could relatively make the effect of liquid flow constrained. We also examined the effect of different initial liquid flow on the microstructure evolution as well as concentration and temperature distribution with heat extraction flux at the boundary, and a secondary arms developing manner transition map was achieved with all the simulation to give an enlightenment of microstructure selection during dendritic structure forming with initial liquid metal flow and heat extraction flux at the boundary. It is suggested that with large heat extraction flux and small initial velocity of initial liquid flow, the microstructure became columnar, and when the heat extraction was large enough, the steady state should be columnar structure. Therefore, it is the competition between forced liquid flow and the heat flux that determines microstructure formation during solidification.

This work was supported by the NPU Foundation of Fundamental Research, China (Grant No. JC201272).

1 Asta M, Beckermann C, Karma A, et al. Solidification microstructures and solid-state parallels: Recent developments, future directions. Acta Mater, 2009, 57: 941–971
2 Chen L Q. Phase-field models for microstructure evolution. Annu Rev Mater Sci, 2002, 32: 113–140
3 Boettinger W J, Warren J A, Beckermann C, et al. Phase-field simu-

lation of solidification. Annu Rev Mater Sci, 2002, 32: 163–194
4 Loginova I S, Singer H M. The phase field technique for modeling multiphase materials. Rep Prog Phys, 2008, 71(10): 106501
5 Steinbach I. Phase-field models in materials science. Modell Simul Mater Sci Eng, 2009, 17(7): 073001
6 Kobayashi R. Modeling and numerical simulations of dendritic crystal-growth. Phys D 1993, 63(3-4): 410–423
7 Wheeler A A, Boettinger W J, Mcfadden G B. Phase-field model for isothermal phase-transitions in binary-alloys. Phys Rev A, 1992, 45: 7424–7439
8 Wheeler A A, Boettinger W J, Mcfadden G B. Phase-field model of solute trapping during solidification. Phys Rev E, 1993, 47: 1893–1909
9 Kim S G, Kim W T, Suzuki T. Interfacial compositions of solid and liquid in a phase-field model with finite interface thickness for isothermal solidification in binary alloys. Phys Rev E, 1998, 58(3): 3316–3323
10 Kim S G, Kim W T, Suzuki T. Phase-field model for binary alloys. Phys Rev E, 1999, 60(6): 7186–7197
11 Karma A. Phase-field formulation for quantitative modeling of alloy solidification. Phys Rev Lett, 2001, 87(11): 115701
12 Karma A, Rappel W J. Quantitative phase-field modeling of dendritic growth in two and three dimensions. Phys Rev E, 1998, 57(4): 4323–4349
13 Beckermann C, Diepers H –J, Steinbach I, et al. Modeling melt convection in phase-field simulations of solidification. J Comput Phys, 1999, 154: 468–496
14 Lan C W, Shih C J. Phase field simulation of non-isothermal free dendritic growth of a binary alloy in a forced flow. J Cryst Growth, 2004, 264: 472–482
15 Nestler B, Choudhury A. Phase-field modeling of multi-component systems. Curr Opin Solid St M, 2011, 15: 93–105
16 Nestler B, Garcke H, Stinner B. Multicomponent alloy solidification: Phase-field modeling and simulations. Phys Rev E, 2005, 71(4): 041609
17 Zhang R J, Li M, Allison J. Phase-field study for the influence of solute interactions on solidification process in multicomponent alloys. Comp Mater Sci, 2010, 47: 832–838
18 Warren J, Boettinger W. Prediction of dendritic growth and microsegregation patterns in a binary alloy using the phase-field method. Acta Metall Mater, 1995, 43: 689–703
19 Loginova I, Amberg G, Agren J. Phase-field simulations of non-isothermal binary alloy solidification. Acta Mater, 2001, 49: 573–581
20 Tang J, Xue X. Phase-field simulation of directional solidification of a binary alloy under different boundary heat flux conditions. J Mater Sci, 2009, 44: 745–753